



Simplification and order reduction of lithium-ion battery model based on porous-electrode theory

Thanh-Son Dao*, Chandrika P. Vyasarayani, John McPhee

Department of Systems Design Engineering, University of Waterloo, 200 University Ave West, Waterloo, Ontario, Canada N2L 3G1

ARTICLE INFO

Article history:

Received 11 July 2011

Received in revised form

13 September 2011

Accepted 13 September 2011

Available online 21 September 2011

Keywords:

Galerkin

Model simplification

Model order reduction

Lithium-ion battery

Porous electrode

Hybrid electric vehicle

ABSTRACT

In this paper, effective and systematic steps in the mathematical simplification and reduction of physics-based lithium-ion (Li-ion) battery models to improve computational efficiency will be presented. The battery model used for simulations is an isothermal model proposed by Newman and Tiedemann [1] and Doyle et al. [2] which incorporates the concentrated solution theory, the porous electrode theory, and the variations in electronic/ionic conductivities and diffusivities. The simplified model is formulated by exploiting the nature of the model and the structure of the governing equations. Simulations show that the simplified model can reduce computational time significantly while still retaining the accuracy compared to the full-order rigorous model.

Crown Copyright © 2011 Published by Elsevier B.V. All rights reserved.

1. Introduction

Due to its advantages such as light weight, low self-discharge rate, and high specific energy, Li-ion batteries have become one of the most popular types of battery in various applications such as portable electronics or electric vehicles. The charge–discharge rate for the lithium-ion battery can vary from 1 to 2C (1C is a discharge rate at nominal battery capacity) to a very fast pulse discharge up to 40–50C over a short time period on the order of 10–20s [3]. In the automotive field, Li-ion batteries are the core of the energy source and storage in new plug-in hybrid electric vehicles (PHEVs) as well as considered in many second generation hybrid electric vehicles (HEVs). The performances of Li-ion batteries play an important role in vehicle energy management. Hence, battery modeling is one of the most important tasks for electric and hybrid vehicle control. This requires a model that can simulate in real-time in order to make them compatible with estimation algorithms embedded in on-board electronic control units. For example, a battery management system in an HEV has to estimate the battery state of charge (SOC) [4–6] in real-time in order control the electrical power com-

ing in and out of the battery as well as to prevent the battery pack from excessive heating.

A full-order battery model, however, is not suitable for real-time applications as it usually takes hours to spatially discretize the system via a finite difference method and solve the system numerically as a collective of differential equations in terms of the field variables. Therefore, a fast and reliable approximate model is required. For automotive applications, a simplified battery model has to be carried out at a good accuracy while ensuring the maximum computational cost reduction to achieve an efficient system management. Subramanian et al. [7–9] developed a real-time simulation model using a combination of perturbation techniques, volume averaging, and intuition-based simplifications. Although they reported that the computational time for their real-time simulation model for a single process was around 100ms, to derive the lower-order model by using this method one needs to carry out preprocessing and have *a priori* knowledge of the behavior of the system under different conditions, which makes their method less flexible than desired. Other methods, including the Chebyshev polynomial method [10,11], residue grouping method [12], proper orthogonal decomposition method [13], and Padé approximation [14] have also been used to derive reduced-order models for Li-ion batteries.

In the methods using Chebyshev polynomials, the state variables are approximated by linear combinations of several Chebyshev polynomials, and then an approximate model is projected onto a subspace formed by these orthogonal Chebyshev polynomials to

* Corresponding author. Tel.: +519 747 2373; fax: +1 519 746 4791.

E-mail addresses: tdao@maplesoft.com (T.-S. Dao),
cpvyasar@gmail.uwaterloo.ca (C.P. Vyasarayani),
mcphee@real.uwaterloo.ca (J. McPhee).

Nomenclature

a_k	specific surface area of electrode k ($k = p, n$) ($\text{m}^2 \text{m}^{-3}$)
brugg_k	Bruggman coefficient of region k ($k = p, n$)
$c_{e,\text{apprx}}$	assumed solution for electrolyte-phase concentration of Li^+ (mol m^{-3})
$c_{e,k}$	electrolyte concentration in region k (mol m^{-3})
$c_{e,k,0}$	initial electrolyte concentration in region k (mol m^{-3})
$c_{s,k}$	concentration of Li^+ ions in the intercalation particle of electrode k (mol m^{-3})
$c_{s,k,0}$	initial concentration of Li^+ ions in the intercalation particle of electrode k (mol m^{-3})
$\bar{c}_{s,k}$	average concentration of Li^+ ions in the intercalation particle of electrode k (mol m^{-3})
$c_{s,k,\text{surf}}$	concentration of Li^+ ions on the surface of intercalation particle of electrode k (mol m^{-3})
D	electrolyte diffusion coefficient ($\text{m}^2 \text{s}$)
$D_{s,k}$	Li^+ ion diffusion coefficient in the intercalation particle of electrode k ($\text{m}^2 \text{s}$)
F	Faraday's constant (C mol^{-1})
I	applied current density (A m^{-2})
J_k	wall-flux of Li^+ on the intercalation particle of electrode k ($\text{mol m}^{-2} \text{s}$)
K_k	intercalation/deintercalation reaction-rate constant of electrode k ($\text{mol mol}^{-1} \text{m}^3$)
L	total thickness of cathode-separator-anode (m)
L_k	thickness of region k (m)
n	negative electrode
N	number of node points for Galerkin's approximation
p	positive electrode
$\bar{q}_{s,k}$	volume-averaged concentration flux of Li^+ ions in the intercalation particle of electrode k ($\text{mol m}^{-3} \text{s}^{-1}$)
r	radial coordinate (m)
R	universal gas constant
R_c	residual function for concentration of Li^+ in electrolyte-phase
$R_{s,k}$	radius of intercalation of electrode k (m)
R_Φ	residual function for electrical potential in electrolyte-phase
s	separator
t_+	Li^+ transference number in the electrolyte
T	absolute temperature (K)
U_k	open-circuit potential of electrode k (V)
x	spatial coordinate (m)

Greek letters

ϵ_k	volume fraction of region k
$\epsilon_{f,k}$	volume fraction of fillers in region k
η_i	time-dependent variable of i 'th basis function for electrolyte-phase concentration (s)
θ_k	dimensionless concentration of Li^+ ions in the intercalation particle of electrode k ($\theta_k = c_{s,k}/c_{s,k,\text{max}}$)
κ	ionic conductivity of electrolyte (S m^{-1})
$\kappa_{\text{eff},k}$	effective ionic conductivity of the electrolyte in region k (S m^{-1})
ρ_i	time-dependent variable of i 'th basis function for electrolyte-phase potential (s)
σ_k	electronic conductivity of solid phase of electrode k (S m^{-1})
$\sigma_{\text{eff},k}$	effective electronic conductivity of solid phase of electrode k (S m^{-1})

Φ_e	electrolyte-phase potential (V)
$\Phi_{e,\text{apprx}}$	assumed solution for electrolyte-phase potential (V)
Φ_s	solid-phase potential (V)

form a reduced-order model, which can then be solved for the unknown coefficients in the truncated expressions. Smith et al. [15] developed a control-oriented one-dimensional (1D) electrochemical model by using the method of residue grouping. Their transfer functions are represented by a truncated series of grouped residues with similar eigenvalues. Cai and White [13] proposed an approach based on proper orthogonal decomposition for tackling the problem by using two steps of approximation: partial differential equation (PDE) discretization and truncation of the number of orthogonal modes. Cai and White showed that the order-reduced model simulated seven times faster than the full-order model for a similar level of accuracy. The electrode-averaging method was used by Speltino et al. [16] who made several simplifications such as neglecting solid concentration distribution and assuming constant electrolyte concentration. As a result, their model simulated fast, but with a heavy loss of information.

In this paper, an efficient method for reducing the order of Li-ion battery models using LiCoO_2 and LiC_6 electrodes derived from the porous electrode theory will be discussed. The simplified model in this paper uses the volume-average integration proposed in Subramanian et al. [7], Wang et al. [17], and Gu et al. [18] for approximating the Li^+ concentration in the solid phase in the electrode material. For modeling the Li^+ concentration and electrical potential in the electrolyte phase, Galerkin's approximation will be used under the assumption of a galvanostatic discharge condition. Maple 14 was used to generate the mathematical model and perform many of the model reductions and simplifications. The paper begins with a brief overview of the intercalated Li-ion models and its mathematical governing equations, followed by a discussion on the use of the volume-average and Galerkin's method to simplify the model. Simulation results and a comparison between the simplified and full-order models will also be provided to demonstrate the effectiveness of the proposed battery model reduction method.

2. Lithium-ion battery model based on porous-electrode theory

2.1. Overview

Most of the current rigorous Li-ion battery models are derived from the porous electrode and concentrated solution theories proposed by Newman and Tiedemann [1] and Doyle et al. [2] which mathematically describe charge/discharge and species transport in the solid and electrolyte phases across a simplified 1D spatial cell structure. This 1D model of a Li-ion battery considers dynamics along only one axis (the horizontal x -axis) and neglects the dynamics along the remaining two axes (y -axis and z -axis) [1,2,19–23]. This approximation is applicable to most cell structures as the length scale of a typical Li-ion cell along the x -axis is on the order of 100 μm , whereas the length scale for the remaining two axes is on the order of 100,000 μm or more [24].

There are four main components in a typical Li-ion cell as shown in Fig. 1: the negative composite electrode connected to the negative terminal of the cell, the positive composite electrode connected to the positive terminal of the cell, the separator, and the electrolyte. The negative electrode contains lithium stored in the lattice sites made from graphite, usually in the form of Li_xC_6 . The positive electrode can have various chemistries, usually a metal oxide or an inter-metallic oxide such as $\text{Li}_x\text{Mn}_2\text{O}_4$ or Li_yCoO_2 . During

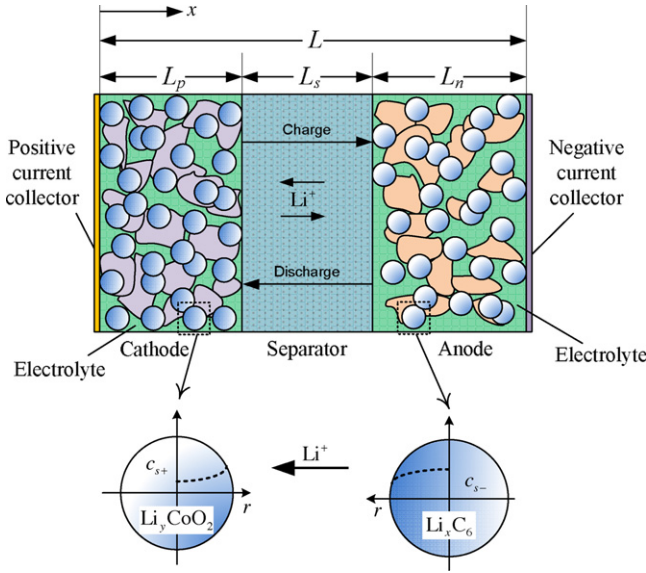


Fig. 1. Anatomy of Li-ion cell.

discharge, Li^+ ions diffuse to the surface of Li_xC_6 active material particles (solid phase) in the negative electrode where they undergo electrochemical reactions and transfer into a liquid electrolyte solution (solution phase). The positively charged Li^+ ions travel through the electrolyte solution via diffusion and ionic conduction to the positive electrode where they react and diffuse towards the inner regions of metal oxide active material particles (solid phase). The process is similar for charging, except that the Li^+ ions move in the opposite direction from the lattice sites in the positive electrode and enter the lattice sites in the negative electrode. This process is called *intercalation* and this is the reason why the Li-ion battery is usually referred to as the *rocking chair model*. The porous separator serves as an electric insulator which forces electrons to follow an opposite path to the ions through an external circuit or load. The separator, however, allows the Li^+ ions to pass through it during battery operation.

2.2. Transport in solid phase

In this section we provide a brief summary of the governing equations for a lithium-ion battery model derived from the porous electrode theory [1,2,19]. According to this theory, the lithium is considered as existing in two disjoint states called phases: the solid phase in the electrode material and the liquid phase in the dissolved state in the electrolyte. In this model, the solid and electrolyte phases are treated as superimposed continua without regard to microstructure. According to Fick's laws of diffusion, the solid-phase Li^+ concentration in a single spherical active material particle can be described as

$$\frac{\partial c_{s,k}(x, r, t)}{\partial t} = \frac{D_{s,k}}{r^2} \frac{\partial}{\partial r} \left(r^2 \frac{\partial c_{s,k}(x, r, t)}{\partial r} \right) \quad (1)$$

with boundary and initial conditions

$$-D_{s,k} \frac{\partial c_{s,k}}{\partial r} \Big|_{r=0} = 0 \quad (2)$$

$$-D_{s,k} \frac{\partial c_{s,k}}{\partial r} \Big|_{r=R_{s,k}} = J_k(x, t) \quad (3)$$

$$c_{s,k}(x, r, 0) = c_{s,k,0} \quad (4)$$

where $k=p$ for the positive electrode and $k=n$ for the negative electrode. The definitions of other symbols can be found in the Nomenclature section.

2.3. Transport in electrolyte

The Li^+ concentration in the electrolyte phase changes due to the changes in the gradient diffusive flow of Li^+ ions. Therefore, it can be shown that

$$\epsilon_k \frac{\partial c_{e,k}(x, t)}{\partial t} = \frac{\partial}{\partial x} \left(D_{\text{eff},k} \frac{\partial c_{e,k}(x, t)}{\partial x} \right) + a_k (1 - t_+) J_k(x, t) \quad (5)$$

In this equation, $k=p$ for the positive electrode, $k=s$ for the separator, and $k=n$ for the negative electrode.

The boundary conditions for Eq. (5) capture the fact that the fluxes of the ions are zero for all time at the current collector. Since the flux is proportional to the concentration gradient at the positive and negative current collectors, we have

$$-D_{\text{eff},p} \frac{\partial c_{e,p}}{\partial x} \Big|_{x=0} = -D_{\text{eff},n} \frac{\partial c_{e,n}}{\partial x} \Big|_{x=L} = 0 \quad (6)$$

We also need four additional boundary conditions at the electrode-separator interface. These boundary conditions are obtained from continuity of the flux and concentration of the electrolyte at the electrode-separator interface as

$$-D_{\text{eff},p} \frac{\partial c_{e,p}}{\partial x} \Big|_{x=L_p^-} = -D_{\text{eff},s} \frac{\partial c_{e,s}}{\partial x} \Big|_{x=L_p^+} \quad (7)$$

$$-D_{\text{eff},s} \frac{\partial c_{e,s}}{\partial x} \Big|_{x=(L_p+L_s)^-} = -D_{\text{eff},n} \frac{\partial c_{e,n}}{\partial x} \Big|_{x=(L_p+L_s)^+} \quad (8)$$

$$c_{e,p} \Big|_{x=L_p^-} = c_{e,s} \Big|_{x=L_p^+} \quad (9)$$

$$c_{e,s} \Big|_{x=(L_p+L_s)^-} = c_{e,n} \Big|_{x=(L_p+L_s)^+} \quad (10)$$

Eq. (5) must also satisfy the initial condition

$$c_{e,k}(x, 0) = c_{e,k,0} \quad (11)$$

The effective diffusion coefficient $D_{\text{eff},k}$ is calculated from a reference coefficient using the Bruggeman relation $D_{\text{eff},k} = D \epsilon_k^{\text{brugg},k}$ that accounts for the tortuous path that Li^+ ions follow through the porous media. In this expression, D is the electrolyte diffusion coefficient which varies with electrolyte concentration. However, D will be approximated as constant within this paper for simplification. The specific electrode surface area can be expressed in terms of the porosity of the electrode as

$$a_k = \frac{3}{R_{s,k}} (1 - \epsilon_k - \epsilon_{f,k}) \quad (12)$$

2.4. Electrical potentials

Charge conservation in the solid phase of each electrode can be described by Ohm's law

$$\sigma_{\text{eff},k} \frac{\partial^2 \Phi_{s,k}(x, t)}{\partial x^2} = a_k F J_k(x, t) \quad (13)$$

with boundary conditions at the current collectors being proportional to applied current density

$$-\sigma_{\text{eff},p} \frac{\partial \Phi_{s,p}}{\partial x} \Big|_{x=0} = -\sigma_{\text{eff},n} \frac{\partial \Phi_{s,n}}{\partial x} \Big|_{x=L} = I \quad (14)$$

$$-\sigma_{\text{eff},p} \frac{\partial \Phi_{s,p}}{\partial x} \Big|_{x=L_p} = -\sigma_{\text{eff},n} \frac{\partial \Phi_{s,n}}{\partial x} \Big|_{x=L_p+L_s} = 0 \quad (15)$$

where the current density I is related to the applied current i and the surface area A of the electrode as $I = i/A$.

The effective electronic conductivity can be expressed in terms of the porosity of the electrode as

$$\sigma_{\text{eff},k} = \sigma_k (1 - \epsilon_k - \epsilon_{f,k}) \quad (16)$$

Combining Kirchhoff's law with Ohm's law in the electrolyte phase yields

$$\begin{aligned} -\sigma_{\text{eff},k} \frac{\partial \Phi_{s,k}(x,t)}{\partial x} - \kappa_{\text{eff},k} \frac{\partial \Phi_{e,k}(x,t)}{\partial x} \\ + \frac{2\kappa_{\text{eff},k}(x,t)RT}{F} (1 - t_+) \frac{\partial \ln c_{e,k}}{\partial x} = I \end{aligned} \quad (17)$$

Both t_+ and $\kappa_{\text{eff},k}$ are usually functions of electrolyte concentration, but t_+ is usually approximated as a constant. The effective diffusion conductivity can be calculated from the Bruggeman relation. In this paper, the conductivity for the liquid/salt/polymer system, consisting of a 2:1 volume mixture of ethylene carbonate (EC) and dimethyl carbonate (DMC), curve-fitted by Doyle et al. [25] will be used in the following form

$$\begin{aligned} \kappa_{\text{eff},k}(x,t) = \epsilon_k^{\text{bruggk}} [4.1253 \times 10^{-2} + 5.007 \times 10^{-4} c_{e,k}(x,t) \\ - 4.7212 \times 10^{-7} c_{e,k}^2(x,t) + 1.5094 \times 10^{-10} c_{e,k}^3(x,t) \\ - 1.6018 \times 10^{-14} c_{e,k}^4(x,t)] \end{aligned} \quad (18)$$

Since we can only measure potential differences, the boundary conditions of $\Phi_{e,k}$ is arbitrary. We set $\Phi_{e,p}(0^+, t) = 0$ at the positive electrode current collector interface. The remaining boundary conditions follow from continuity of $\Phi_{e,k}$ that

$$-\kappa_{\text{eff},p} \frac{\partial \Phi_{e,p}}{\partial x} \Big|_{x=0} = -\kappa_{\text{eff},n} \frac{\partial \Phi_{e,n}}{\partial x} \Big|_{x=L} = 0 \quad (19)$$

$$-\kappa_{\text{eff},p} \frac{\partial \Phi_{e,p}}{\partial x} \Big|_{x=L_p^-} = -\kappa_{\text{eff},s} \frac{\partial \Phi_{e,s}}{\partial x} \Big|_{x=L_p^+} \quad (20)$$

$$-\kappa_{\text{eff},s} \frac{\partial \Phi_{e,s}}{\partial x} \Big|_{x=(L_p+L_s)^-} = -\kappa_{\text{eff},n} \frac{\partial \Phi_{e,n}}{\partial x} \Big|_{x=(L_p+L_s)^+} \quad (21)$$

It should be noted that the solid-phase potential $\Phi_{e,k}(x,t)$ and current density $J_k(x,t)$ do not exist in the separator region and, therefore, the terms containing these variables are eliminated from Eqs. (5) and (17) for the separator region.

2.5. Butler–Volmer kinetics

The molar flux $J_k(x,t)$ depends on the concentration $c_{s,k}$ of Li^+ in the electrode k , the concentration of Li^+ in the electrolyte, and the intercalation over-potential $\mu_{s,k}(x,t)$ through the Butler–Volmer equation [21]. This over-potential can be described as

$$\mu_{s,k}(x,t) = \Phi_{s,k}(x,t) - \Phi_{e,k}(x,t) - U_k(\theta_k(x,t)) \quad (22)$$

where the open-circuit potential equations for positive (LiCoO_2) and negative (LiC_6) electrodes were curve-fitted from experimental data [2] and have the form

$$U_p(x,t) = \frac{-4.656 + 88.669\theta_p^2 - 401.119\theta_p^4 + 342.909\theta_p^6 - 462.471\theta_p^8 + 433.434\theta_p^{10}}{-1.0 + 18.933\theta_p^2 - 79.532\theta_p^4 + 37.311\theta_p^6 - 73.083\theta_p^8 + 95.96\theta_p^{10}} \quad (23)$$

$$\begin{aligned} U_n(x,t) = 0.7222 + 0.1387\theta_n + 0.029\theta_n^{0.5} - \frac{0.0172}{\theta_n} + \frac{0.0019}{\theta_n^{1.5}} \\ + 0.2808 \exp(0.90 - 15\theta_n) - 0.7984 \\ \times \exp(0.4465\theta_n - 0.4108) \end{aligned} \quad (24)$$

with θ_k being given by

$$\theta_k(x,t) = \frac{c_{s,k,\text{surf}}(x,t)}{c_{s,k,\text{max}}} \quad (25)$$

The Butler–Volmer equation describing the relationship between the current density, concentrations, and over-potential is given by Newman and Thomas-Aleya [21]

$$\begin{aligned} J_k(x,t) = K_k (c_{s,k,\text{max}} - c_{s,k,\text{surf}})^{0.5} (c_{s,k,\text{surf}})^{0.5} c_{e,k}^{0.5}(x,t) \\ \times \left[\exp\left(\frac{0.5F}{RT} \mu_{s,k}(x,t)\right) - \exp\left(-\frac{0.5F}{RT} \mu_{s,k}(x,t)\right) \right] \end{aligned} \quad (26)$$

In summary, the equations that need to be solved are (1), (5), (13), (17), (23), (24), and (26). The battery model is, therefore, a mixed system with 14 nonlinear partial differential algebraic equations (PDAEs) with 14 unknowns, which are: $c_{s,p}$, $c_{s,n}$, $c_{e,p}$, $c_{e,s}$, $c_{e,n}$, $\Phi_{s,p}$, $\Phi_{s,n}$, $\Phi_{e,p}$, $\Phi_{e,s}$, $\Phi_{e,n}$, U_p , U_n , J_p , and J_n .

3. Model simplification

3.1. Solid phase concentration

For the solid-phase concentration, we are only interested in the solid-phase Li^+ concentration on the surfaces of the lithium particles for electrochemical behaviors and average concentration for state of charge calculation. Therefore, it is desirable to only extract the equations for these two quantities without having to solve the entire two PDEs for the solid-phase concentration. In the process, the dependencies on the radial dimension r are eliminated.

Simplified, yet accurate, equations for surface and average concentrations can be obtained using the polynomial approximation and volume-average integration suggested by Subramanian et al. [7]. The procedures can be started by choosing a concentration profile inside a particle at a known x position. In this case, we choose a three-variable model

$$c_{s,k}(r,t) = a(t) + b(t) \frac{r^2}{R_{s,k}^2} + d(t) \frac{r^4}{R_{s,k}^4} \quad (27)$$

Substituting the above polynomial function into Eq. (1) yields

$$\frac{da(t)}{dt} + \frac{r^2}{R_{s,k}^2} \frac{db(t)}{dt} + \frac{r^4}{R_{s,k}^4} \frac{dd(t)}{dt} - 2 \frac{D_{s,k}}{R_{s,k}^2} \left(3b(t) + 10 \frac{r^2}{R_{s,k}^2} d(t) \right) = 0 \quad (28)$$

This equation automatically satisfies the boundary condition at $r=0$, therefore we only need to make sure the equation also satisfies the second boundary condition at $r=R_{s,k}$. This corresponds to

$$\frac{2D_{s,k}b(t)}{R_{s,k}} + \frac{4D_{s,k}d(t)}{R_{s,k}} = -J_k(t) \quad (29)$$

The three unknowns $a(t)$, $b(t)$, and $d(t)$ can be solved in terms of the average concentration $\bar{c}_{s,k}(t)$, surface concentration $c_{s,k,\text{surf}}(t)$, and an auxiliary term called volume-averaged concentration flux

$\bar{q}_{s,k}(t)$ as (detailed solution can be found in Subramanian et al. [7])

$$\begin{aligned} a(t) &= \frac{39}{4} c_{s,k,\text{surf}}(t) - 3\bar{q}_{s,k}(t) - \frac{35}{4} \bar{c}_{s,k}(t) \\ b(t) &= -35c_{s,k,\text{surf}}(t) + 10\bar{q}_{s,k}(t) + 35\bar{c}_{s,k}(t) \\ d(t) &= \frac{105}{4} c_{s,k,\text{surf}}(t) - 7\bar{q}_{s,k}(t) - \frac{105}{4} \bar{c}_{s,k}(t) \end{aligned} \quad (30)$$

The solid-phase concentration now can be expressed in terms of the surface concentration and average concentration by substituting (30) into (28)

$$c_{s,k}(r, t) = \frac{39}{4} c_{s,k,surf}(t) - 3\bar{q}_{s,k}(t)R_{s,k} - \frac{35}{4} \bar{c}_{s,k}(t)[-35c_{s,k,surf}(t) + 10\bar{q}_{s,k}(t)(t)R_{s,k} + 35\bar{c}_{s,k}(t)] \frac{r^2}{R_{s,k}^2} + \left[\frac{105}{4} c_{s,k,surf}(t) - 7\bar{q}_{s,k}(t)R_{s,k} - \frac{105}{4} \bar{c}_{s,k}(t) \right] \frac{r^4}{R_{s,k}^4} \quad (31)$$

By applying the volume-average integration for the original PDE and its differentiation, we can obtain the two ordinary differential equations (ODEs)

$$\frac{d}{dt} \bar{c}_{s,k}(t) + 3 \frac{J_k(t)}{R_{s,k}} = 0 \quad (32)$$

$$\frac{d}{dt} \bar{q}_{s,k}(t) + 30 \frac{D_{s,k}}{R_{s,k}^2} \bar{q}_{s,k}(t) + \frac{45}{2} \frac{J_k(t)}{R_{s,k}^2} = 0 \quad (33)$$

The third equation can be obtained by evaluating the boundary condition at $r=R_{s,k}$. This gives

$$35 \frac{D_{s,k}}{R_{s,k}} [c_{s,k,surf}(t) - \bar{c}_{s,k}(t)] - 8D_{s,k} \bar{q}_{s,k}(t) = -J_k(t) \quad (34)$$

Solving the ODEs in (32), (33), and (34) simultaneously using a numerical solver gives the surface and average concentration profiles for the Li^+ concentration in solid phase.

The next sections will present the main contribution of this paper, the use of Galerkin’s method and analytical techniques to reduce the PDEs describing the electrolyte phase concentration ($c_{e,k}$) and electrical potential equations ($\Phi_{s,k}$ and $\Phi_{e,k}$) to ODEs.

3.2. Electrolyte phase concentration

The Li^+ concentration in the electrolyte phase can be approximated by applying Galerkin’s approximation to Eq. (5). The first step of the Galerkin method is to choose a basis function that satisfies all the boundary conditions (6)–(7), and (8). For simplicity, we approximate the three PDEs across three regions (i.e., anode, separator, and cathode regions) by one single PDE with the x -dimension spanning from 0 to L

$$\epsilon \frac{\partial c_e(x, t)}{\partial t} = \frac{\partial}{\partial x} \left(D_{eff} \frac{\partial c_e(x, t)}{\partial x} \right) + a(1 - t_+)J \quad (35)$$

The only differences in the three parts of this PDE are the physical parameters in the three regions and the boundary conditions at the cathode-separator and separator-anode interfaces. This can be taken into account when applying the least-square integration and will be shown in the next steps.

Using the criteria discussed above, we can choose the sinusoidal basis function

$$\alpha_i(x) = \cos \left(\frac{i\pi x}{L} \right) \quad (36)$$

We can then define the assumed solution as the sum of the basis functions in the form

$$c_{e,approx}(x, t) = c_{e,0} + \sum_{i=1}^N [\alpha_i(x)\eta_i(t)] = c_{e,0} + \sum_{i=1}^N \left[\cos \left(\frac{i\pi x}{L} \right) \eta_i(t) \right] \quad (37)$$

where N is the number of terms or node points. Each term of the sum is the product of a given basis function and an *unknown* function of

time $\eta_i(t)$. It can be easily verified that the assumed solution function satisfies the boundary conditions as well. The $c_{e,0}$ is included to ensure the assumed solution satisfies the initial condition given in Eq. (11). The first two terms in the assumed solution in (37) give a straight line function of x that interpolates the boundary values. The terms in the summation contribute nonlinearities to the solution.

Substituting the assumed solution into the PDE in (35) gives

$$R_c(x, t) = \epsilon \sum_{i=1}^N \left(\alpha_i(x) \frac{d\eta_i(t)}{dt} \right) - D_{eff} \sum_{i=1}^N \left(\frac{d^2 \alpha_i(x)}{dx^2} \eta_i(t) \right) + a(1 - t_+)J \approx 0 \quad (38)$$

This function is known as the *residual*. In the Galerkin method, we replace the condition that the residual should be approximately zero by the condition that the residual should be orthogonal to the set of basis functions. That is, for $i = 1, \dots, N$ we multiply the residual by the basis function $\cos(i\pi x/L)$ and integrate over x , and set the result to zero. For convenience, we define the following operator:

Definition 1. Inner product Consider the real functions whose domain is the closed interval $[a, b]$. We define the inner product of two functions $f(x, t)$ and $g(x)$ as follows

$$\langle f, g \rangle_a^b = \int_a^b f(x, t)g(x)dx \quad (39)$$

Using this inner product operator, we can write the integration as follows

$$\langle R_c, \alpha_i \rangle_{0^p}^{L_p} + \langle R_c, \alpha_i \rangle_{L_p}^{L_p+L_s} + \langle R_c, \alpha_i \rangle_{L_p+L_s}^{L_p+L_s} = 0, \quad i = 1, \dots, N \quad (40)$$

In the above equation, we substitute ($\epsilon = \epsilon_n, D_{eff} = D_{eff,n}, a = a_n$) into the first term, ($\epsilon = \epsilon_s, D_{eff} = D_{eff,s}, a = a_s$) into the second term, and ($\epsilon = \epsilon_p, D_{eff} = D_{eff,p}, a = a_p$) into the last term. In this way we obtain a set of N linear ODEs that only contains the time-dependent functions $\eta_i(t)$. These ODEs can be expressed using the matrix form

$$\begin{pmatrix} \dot{\eta}_1(t) \\ \dot{\eta}_2(t) \\ \dots \\ \dot{\eta}_N(t) \end{pmatrix} = -[A_c] \begin{pmatrix} \eta_1(t) \\ \eta_2(t) \\ \dots \\ \eta_N(t) \end{pmatrix} + [B_c] \quad (41)$$

where $[A_c]$ and $[B_c]$ are $N \times N$ matrices whose constant elements are obtained during the integration process in (40).

3.3. Solid phase potential

For simplification, we assume that the current density J_k is constant. Based on this assumption, we can solve for the closed-form solution for the solid-phase potential. Substituting $J_p = I/a_pFL_p$ into Eq. (13) and integrating Eq. (13) twice over x gives a quadratic equation for the positive solid-phase potential

$$\Phi_{s,p}(x, t) = -\frac{1}{2} \frac{a_p F J_p x^2}{\sigma_{eff,p}} + g_p(t)x + f_p(t) \quad (42)$$

where $g_p(t)$ and $f_p(t)$ are the quantities produced by the indefinite integration. The expression for $g_p(t)$ can be determined by evaluating Eq. (42) at the boundary condition at $x=0$ shown in Eq. (14). This gives

$$g_p(t) = \frac{I}{\sigma_{eff,p}} \quad (43)$$

which, when substituted into Eq. (42) yields

$$\Phi_{s,p}(x, t) = -\frac{1}{2} \frac{a_p F J_p x^2}{\sigma_{eff,p}} + \frac{I}{\sigma_{eff,p}} x + f_p(t) \quad (44)$$

Similarly, by integrating Eq. (13) twice over x and evaluating its result at the boundary condition at $x=L$ the closed form solution for the solid-phase potential on the negative electrode can be obtained as

$$\Phi_{s,n}(x, t) = -\frac{1}{2} \frac{a_n F J_n x^2}{\sigma_{\text{eff},n}} + \frac{a_n F J_n (L_s + L_p)}{\sigma_{\text{eff},n}} x + f_n(t) \quad (45)$$

From Eqs. (44) and (45), instead of solving for $\Phi_{s,p}(x, t)$ and $\Phi_{s,n}(x, t)$, we can now substitute these two quantities into the electrolyte phase potential (discussed in the next section) and Butler–Volmer Eq. (26) and, at a known x position, we can solve for the two unknowns $f_p(t)$ and $f_n(t)$.

3.4. Electrolyte phase potential

Similar to the process used for the electrolyte-phase concentration, we can apply Galerkin method to the electrolyte phase potential to obtain approximate ODEs for this PDE. In a similar manner, we use a single PDE to represent the three PDEs in three different regions as follows

$$-\sigma_{\text{eff}} \frac{\partial \Phi_s(x, t)}{\partial x} - \kappa_{\text{eff}} \frac{\partial \Phi_e(x, t)}{\partial x} + \frac{2\kappa_{\text{eff}}(x, t)RT}{F} \times (1 - t_+) \frac{\partial \ln c_e(x, t)}{\partial x} = I \quad (46)$$

In a similar manner, we can choose the basis function $\beta_i(x) = \cos(i\pi x/L)$ and write the approximate function as

$$\Phi_{e,\text{apprx}}(x, t) = \sum_{i=1}^N [\beta_i(x) \rho_i(t)] = \sum_{i=1}^N \left[\cos\left(\frac{i\pi x}{L}\right) \rho_i(t) \right] \quad (47)$$

and then the residual by substituting Eq. (47) into Eq. (46)

$$R_\phi(x, t) = -\sigma_{\text{eff}} \frac{\partial \Phi_s(x, t)}{\partial x} + \kappa_{\text{eff}} \sum_{i=1}^N \left(\frac{d\beta_i(x)}{dx} \rho_i(t) \right) + \frac{2\kappa_{\text{eff}}(x, t)RT}{F} (1 - t_+) \frac{\partial \ln c_e(x, t)}{\partial x} - I \approx 0 \quad (48)$$

The set of N equations can be obtained by the following integration

$$\langle R_\phi, \beta_i \rangle_0^{L_p} + \langle R_\phi, \beta_i \rangle_{L_p}^{L_p+L_s} + \langle R_\phi, \beta_i \rangle_{L_p+L_s}^L = 0, \quad i = 1, \dots, N \quad (49)$$

In the above equation, we substitute appropriate parameters for each region and use Eq. (44) for the positive electrode solid-phase potential and Eq. (45) for the negative electrode solid-phase potential. The electrolyte-phase concentration $c_e(x, t)$ inside the $\ln(\cdot)$ function can also be replaced by its approximate expression in Eq. (37) and evaluated at the nodal x positions. Doing so we obtain a set of N nonlinear algebraic equations (there are no ODEs because there are no time derivatives in the original PDE) containing a mixture of the time-dependent functions $\rho_i(t)$, $\eta_i(t)$, $f_p(t)$, and $f_n(t)$ in the following matrix form

$$[A_\phi(\eta_i(t))] \begin{pmatrix} \rho_1(t) \\ \rho_2(t) \\ \dots \\ \rho_N(t) \end{pmatrix} + [B_\phi(\eta_i(t), \frac{1}{\eta_i(t)})] \begin{pmatrix} \eta_1(t) \\ \eta_2(t) \\ \dots \\ \eta_N(t) \end{pmatrix} + [D_\phi] \begin{pmatrix} f_p(t) \\ f_p(t) \\ \dots \\ f_n(t) \end{pmatrix} + [E_\phi] \quad (50)$$

in which the inverse of $\eta_i(t)$ appears due to the differentiation of the logarithm terms. The first two square matrices are the functions of

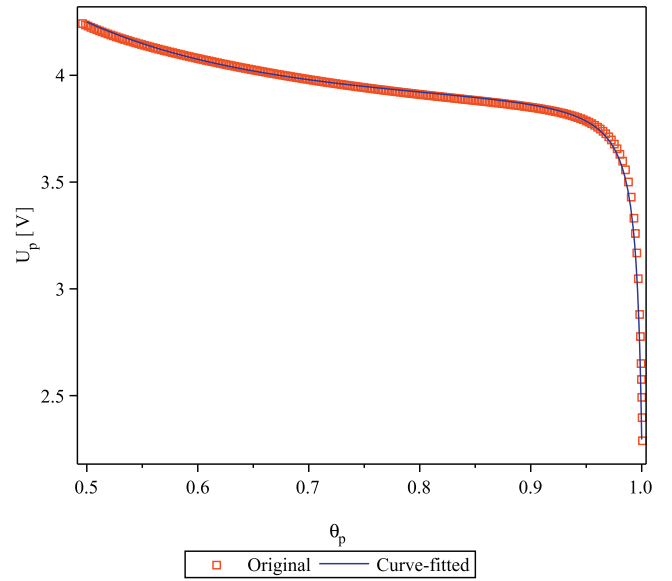


Fig. 2. Open-circuit voltage for positive electrode.

$\eta_i(t)$ which come from the integration of $\kappa(x, t)$ and $\ln c_e(x, t)$ while the last two matrices are constant.

3.5. Open-circuit voltage equations

The order of the open-circuit voltage equations for the two electrodes given in (23) and (24) can be reduced to increase computational speed by eliminating the high-order terms using a nonlinear curve-fitting technique. After trying different function combinations, we have come up with simpler forms for these functions. The original open-circuit equations can be replaced by the following simple expressions

$$U_p(t) = \frac{-4.875 + 5.839\theta_p - 1.507\theta_p^3 + 0.531\theta_p^5}{\theta_p - 1.005} \quad (51)$$

$$U_n(t) = 0.15 - 0.10\theta_n + \frac{0.00778}{\theta_n} \quad (52)$$

For comparison, the open-circuit voltages in Eqs. (51) and (52) plotted along side with the original equations are shown in Figs. 2 and 3.

3.6. Solving battery equations

Using the procedures discussed above, we obtain a set of $2N+10$ differential algebraic equations (DAEs) that consists of the dependent variables $\eta_i(t)$, $\rho_i(t)$, $f_p(t)$, $f_n(t)$, $U_p(t)$, $U_n(t)$, $\bar{c}_{s,k}(t)$, $\bar{q}_{s,k}(t)$, $c_{s,k,\text{surf}}(t)$ and two independent variables x and t . These variables correspond to the differential and algebraic expressions in (32)–(34), (41), (50)–(52), and one (26) for each of J_p and J_n with the assumption of uniform reaction rate.

We are mainly interested in calculating the battery voltage $V_{\text{cell}}(t)$ given by the following relation

$$V_{\text{cell}}(t) = \Phi_{s,p}(0, t) - \Phi_{s,n}(L, t) \quad (53)$$

This equation results in two sets of DAEs evaluated at $x=0$ and $x=L$. These DAEs are only functions of time and can be solved numerically if the initial conditions are known.

The initial conditions for all variables are needed to solve the system. For the solid-phase concentration variables $\bar{c}_{s,k}(t)$ and $c_{s,k,\text{surf}}(t)$ the initial conditions are known and are equal to $c_{s,k,0}$. The initial value for the third variable $\bar{q}_{s,k}(t)$ in the solid-phase concentration equations can be determined by evaluating Eqs. (32)–(34)

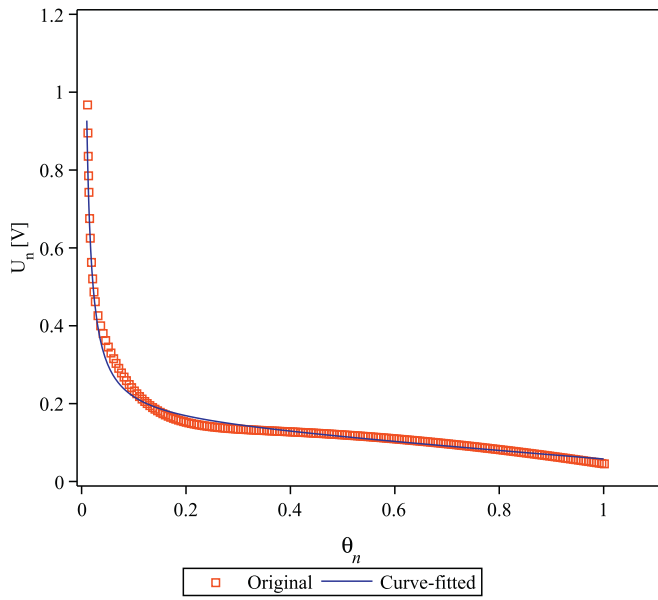


Fig. 3. Open-circuit voltage for negative electrode.

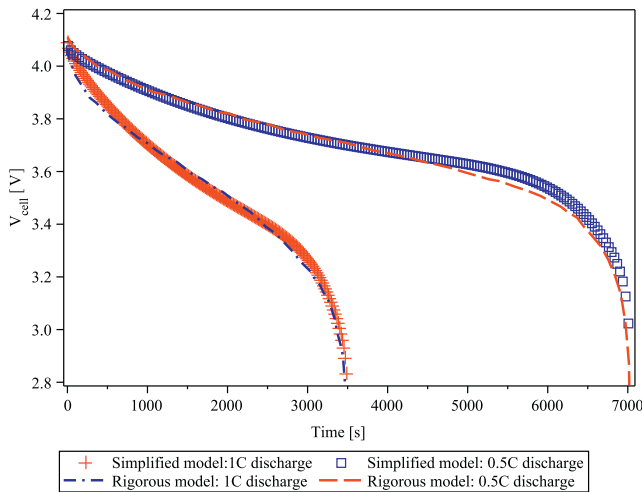


Fig. 4. Discharge curves for 1C (30 A m⁻²) and 0.5C rates at N=4.

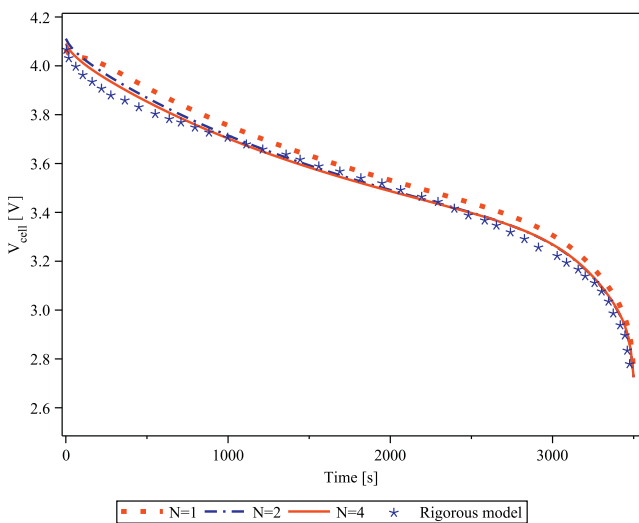


Fig. 5. 1C discharge voltage curve comparison between the rigorous model and the simplified model at different number of node points.

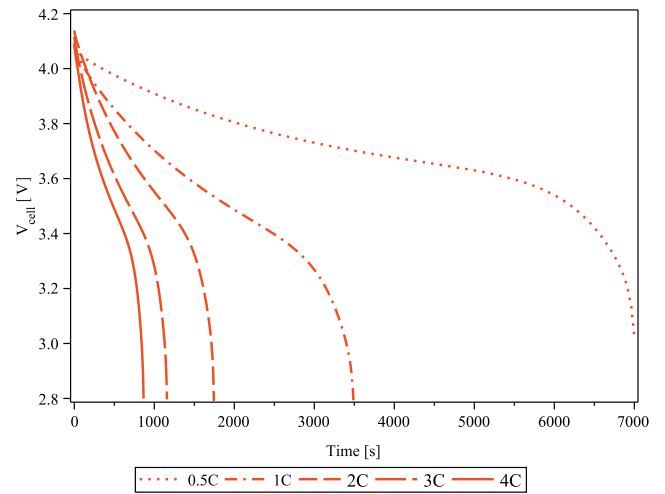


Fig. 6. Voltage curves for different discharge rates at N=4.

at $\bar{c}_{s,k}(t) = c_{s,k,\text{surf}}(t) = c_{s,k,0}$. In the DAEs obtained from Galerkin's method in Eqs. (41) and (50), we can solve for the initial conditions for $\eta_i(t)$ and $\rho_i(t)$ by first expanding the initial conditions of the assumed solution in terms of a series solution as

$$w_{\text{apprx}}(x, 0) = \sum_{i=1}^N \Gamma_i(x) \xi_i(0) \quad (54)$$

where $\Gamma(x)$ represents the x -dependent part and $\xi(0)$ represents the initial value of the time-dependent part of Eqs. (41) and (50). We can then obtain the values for $\xi(0)$ (i.e., $\eta_i(0)$ or $\rho_i(0)$) by multiplying the above equation with $\Gamma(x)$ and solving the resulting equations

$$\langle w_{\text{apprx}}(x, 0), \Gamma_i(x) \rangle_0^L - \sum_{j=1}^N \xi_j(0) \langle \Gamma_j(x), \Gamma_i(x) \rangle_0^L = 0, \quad i = 1, \dots, N \quad (55)$$

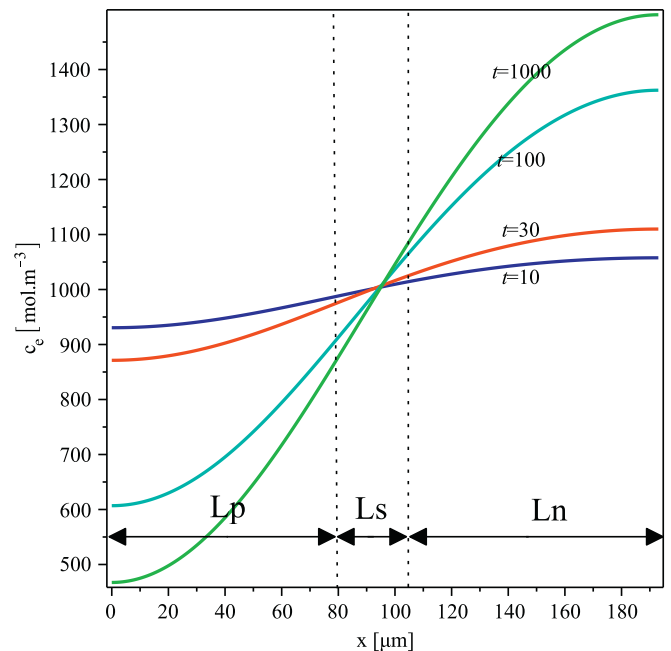


Fig. 7. Electrolyte-phase concentration of Li⁺ at the current collector and electrode-separator interfaces at 1C discharge rate.

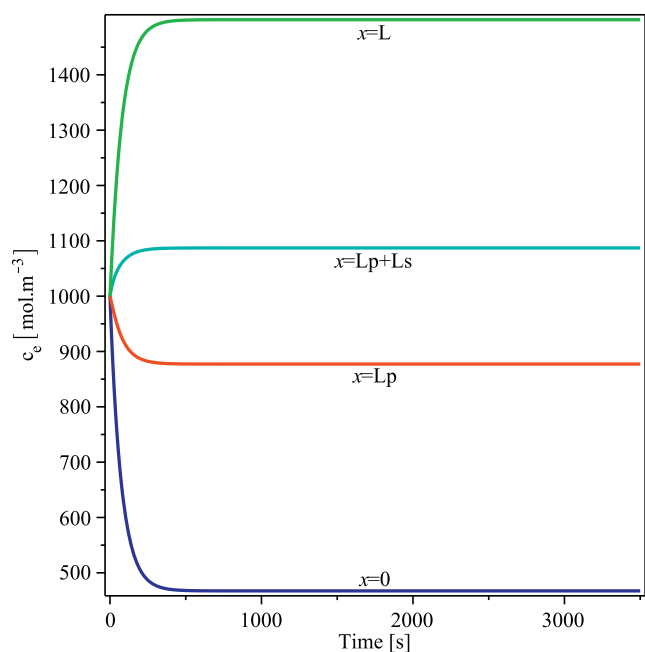


Fig. 8. Electrolyte-phase concentration of Li^+ at the current collector and electrode-separator interfaces at 1 C discharge rate.

The initial values for the remaining variables $f_p(t)$, $f_n(t)$, $U_p(t)$, and $U_n(t)$ can be obtained by solving all the algebraic expressions with the known initial conditions.

3.7. Simulation results

Discharge behavior is the primary goal of the simulation performed in this paper. The parameters used in the simulations are obtained from Subramanian et al. [9] and are listed in Table A.1. Fig. 4 shows complete discharge voltage curves at 1 C (30 A m^{-2}) and 0.5 C rates of galvanostatic discharge with the number of node points being $N=4$. Fig. 5 compares the voltage curves resulting from the simplified model at different numbers of node points and the full-order rigorous model solved using a finite difference approach at 1 C discharge rate. The plots for the rigorous model were extracted from the work done by Subramanian et al. [9]. It can be seen that even with the number of node points $N=2$, there is a good agreement between the simplified model and the rigorous model and this was improved further at $N=4$. The number of DAEs that are solved simultaneously using Galerkin's approach is $2N+10$ while the rigorous model needs to be discretized into hundreds of

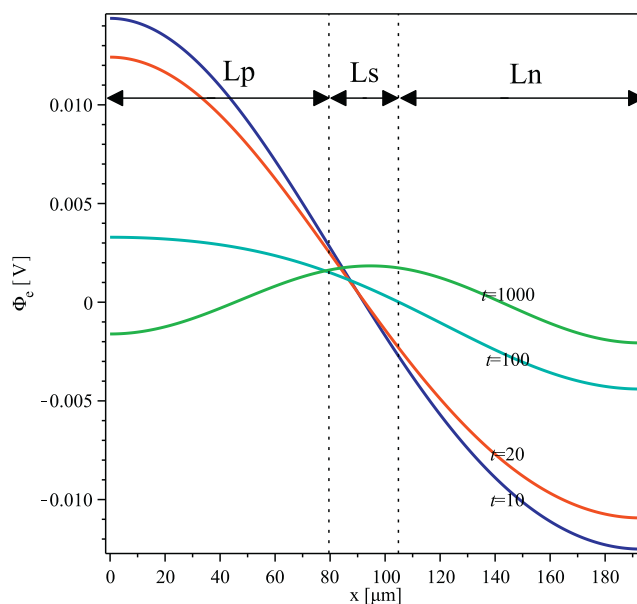


Fig. 9. Electrolyte-phase potential at the current collector and electrode-separator interfaces at 1 C discharge rate.

equations to obtain a good accuracy. For example, the results for the full-order model shown in Figs. 4 and 5 were obtained by discretizing the PDEs governing the battery model into 600 DAEs shown in the work of [9]. The simplification also results in a great reduction in simulation time for the approximate model. Specifically, it took 94 ms on average to simulate the system at $N=4$ in Maplesoft's flagship software, Maple 14, on a Dell™ OptiPlex 2.9 GHz desktop computer.

The battery potentials for low and high discharge rates are plotted in Fig. 6. Since no results for high-rate discharge that can be used for comparison were reported in the work by Subramanian et al. [9], the consistency between the results over a range of discharge rates shown in Fig. 6 indicates that the simplified model works as expected.

The simplified model is also able to predict the other electrochemical variables such as the concentration of Li^+ in the electrolyte (c_e) as shown in Figs. 7 and 8, and the electrolyte phase potential (Φ_e) as shown in Fig. 9. The electrolyte-phase concentration and potential determined by the simplified model are plotted at $t=10$, $t=20$, $t=100$, and $t=1000$. It can be seen that there is no discontinuity in the slopes of the curves at the positive electrode-separator and separator-negative electrode boundaries because the

Table A.1
Battery parameters.

Symbol	Unit	Positive electrode	Separator	Negative electrode
σ_k	S m^{-1}	100		100
$\epsilon_{f,k}$		0.025		0.0326
ϵ_k		0.385	0.724	0.485
brugg		4	4	4
$D_{s,k}$	$\text{m}^2 \text{ s}^{-1}$	1×10^{-14}		3.9×10^{-14}
D	$\text{m}^2 \text{ s}^{-1}$	7.5×10^{-10}	7.5×10^{-10}	7.5×10^{-10}
K_k	$\text{mol} (\text{mol m}^{-3})^{-1.5}$	2.344×10^{-11}		5.0307×10^{-11}
$c_{s,k,\text{max}}$	mol m^{-3}	51,554		30,555
$c_{s,k,0}$	mol m^{-3}	$0.4955 \times 51,554$		$0.8551 \times 30,555$
$c_{e,0}$	mol m^{-3}	1000	1000	1000
$R_{s,k}$	m	2.0×10^{-6}		2.0×10^{-6}
L_k	m	80×10^{-6}	25×10^{-6}	88×10^{-6}
R_{SEI}	$\Omega \text{ m}^2$			0
t_+		0.363	0.363	0.363
F	C mol^{-1}		96,487	
R	$\text{J mol}^{-1} \text{ K}^{-1}$		8.314	

three PDEs in three regions are approximated by only one PDE as shown in Eqs. (35) and (46). This approximation, however, only results in a little loss of information while the computational time is reduced since the number of equations that are solved simultaneously is reduced by a factor of three.

4. Conclusion

In this paper, we have presented a method for simplifying rigorous Li-ion battery models. The isothermal model used for simplification is based on the first principles of the porous electrode and concentrated solution theories. Besides utilizing the nature of the battery equations, a combination of several techniques such as volume-averaging, Galerkin's method, and curve-fitting have been used to achieve an approximate model that can simulate in milliseconds without a significant loss in accuracy compared to the full-order rigorous model.

The paper only discusses simulation results for discharging behaviors. However, it is clear that the method presented in this paper is also directly applicable for charging as it only changes the sign of the applied current density.

Acknowledgements

Financial support for this research has been provided by the Natural Sciences and Engineering Research Council of Canada (NSERC), Toyota, and Maplesoft.

Appendix A. Battery parameters used in simulations

See Table A.1

References

- [1] J. Newman, T. William, *AIChE J.* 21 (1) (1975) 25–41.
- [2] M. Doyle, T. Fuller, J. Newman, *J. Electrochem. Soc.* 140 (1993) 1526–1533.
- [3] K. Smith, C.Y. Wang, *J. Power Sources* 161 (2006) 628–639.
- [4] T.-S. Dao, A. Seaman, J. McPhee, *Proceedings of the 5th Asian Conference on Multibody Dynamics*, 2010.
- [5] D.D. Domenico, G. Fiengo, A. Stefanopoulou, *Proceedings of the 17th IEEE International Conference on Control Applications*, 2008, pp. 702–707.
- [6] D.D. Domenico, A. Stefanopoulou, G. Fiengo, *J. Dyn. Syst. Meas. Control* 132 (2010).
- [7] V.R. Subramanian, V.D. Diwakar, D. Tapriyal, *J. Electrochem. Soc.* 152(10)(2005) A2002–A2008.
- [8] V.R. Subramanian, V. Boovaragavan, V.D. Diwakar, *Electrochem. Solid State Lett.* 10 (11) (2007) A255–A260.
- [9] V.R. Subramanian, V. Boovaragavan, V. Ramadesigan, M. Arabandi, *J. Electrochem. Soc.* 156 (4) (2009) A260–A271.
- [10] M. Golubitsky, D.G. Schaeffer, *Singularities and Groups in Bifurcation Theory*, vol. 1, Springer-Verlag, Berlin, 1984.
- [11] B. Bhikkaji, T. Soderstrom, *Energy Build.* 33 (8) (2001) 769–781.
- [12] K.A. Smith, C.D. Rahn, C.Y. Wang, *IEEE Trans. Control Syst. Technol.* 18 (3) (2010) 654–663.
- [13] L. Cai, R.E. White, *J. Electrochem. Soc.* 156 (3) (2009) A154–A161.
- [14] J.C. Forman, S. Bashash, J.L. Stein, H.K. Fathy, *J. Electrochem. Soc.* 158 (2) (2011) A93–A101.
- [15] K.A. Smith, C.D. Rahn, C.Y. Wang, *Energy Convers. Manage.* 48 (2007) 2565–2578.
- [16] C. Speltino, D. Di Domenico, G. Fiengo, A. Stefanopoulou, *Proceedings of the Joint 48th IEEE Conference on Decision and Control and the 28th Chinese Control Conference*, Shanghai, China, 2009, pp. 3276–3281.
- [17] C.Y. Wang, W.B. Gu, *J. Electrochem. Soc.* 145 (10) (1998) 3407–3417.
- [18] W.B. Gu, C.Y. Wang, B.Y. Liaw, *J. Electrochem. Soc.* 145 (10) (1998) 3418–3427.
- [19] T. Fuller, M. Doyle, J. Newman, *J. Electrochem. Soc.* 141 (1994) 1–10.
- [20] K. Thomas, J. Newman, R. Darling, *Advances in Lithium-Ion Batteries: Mathematical Modeling of Lithium Batteries*, Springer-Verlag, New York, 2002.
- [21] J. Newman, K.E. Thomas-Aleya, *Electrochemical Systems*, 3rd ed., John Wiley & Sons Inc., 2004.
- [22] I.J. Ong, J. Newman, *J. Electrochem. Soc.* 146 (12) (1999) 4360–4365.
- [23] P.M. Gomadam, J.W. Weidner, R.A. Dougal, R.E. White, *J. Power Sources* 110 (2002) 267–284.
- [24] N.A. Chaturvedi, R. Klein, J. Christensen, J. Ahmed, A. Kojic, *IEEE Control Syst. Mag.* (2010).
- [25] M. Doyle, J. Newman, A.S. Gozdz, C.N. Schmutz, J.M. Tarascon, *J. Electrochem. Soc.* 143 (6) (1996) 1890–1903.